International Journal of Refractory Metals and Hard Materials 111 (2023) 106099

Contents lists available at ScienceDirect

International Journal of Refractory Metals and Hard Materials

journal homepage: www.elsevier.com/locate/IJRMHM

Testing length-scale considerations in mechanical characterization of WC-Co hardmetal produced via binder jetting 3D printing

L. Cabezas [a,b,*], C. Berger [c], E. Jiménez-Piqué [a,b], J. Pötschke [c], L. Llanes [a,b]

[a] CIEFMA, Department of Materials Science and Engineering, Universitat Politècnica de Catalunya - BarcelonaTech, Campus Diagonal Besòs-EEBE, 08019 Barcelona, Spain
[b] Barcelona Research Center in Multiscale Science and Engineering, Universitat Politècnica de Catalunya - BarcelonaTech, Campus Diagonal Besòs, 08019 Barcelona, Spain
[c] Fraunhofer Institute for Ceramic Technologies and Systems IKTS, 01277 Dresden, Germany

ARTICLE INFO

Keywords:
Binder jetting
Additive manufacturing
WC-Co hardmetals
Vickers hardness
Scratch testing
Deformation/fracture micromechanisms

ABSTRACT

The extreme versatility of additive manufacturing (AM) as processing technology results in "AMed pieces" with intrinsic characteristics linked to the shaping route followed, which are also key for defining mechanical integrity. The latter requires validation by measuring the mechanical properties, at both macroscopic (global) and microscopic (local) levels; and thus, consideration of specific testing length-scale aspects. This work aims to study the correlation between microstructure and mechanical properties for a WC-12%$_{wt.}$Co hardmetal grade produced via binder jetting 3D printing (BJT) and subsequent sintering. In doing so, macro- and micro- Vickers hardness as well as scratch tests, using different loads and indenter tips, are conducted. It is found that studied samples processed by means of BJT exhibit a microstructure consisting of a relatively wide carbide size distribution, including a significant volume fraction (higher than 15%) of carbides larger than 3 μm. This is a direct consequence of the relatively high sintering temperature needed for getting full dense specimens, when manufactured following this AM route. Meanwhile, mechanical properties are found to be isotropic, with hardness and scratch resistance values falling within ranges of those expected for hardmetals with similar binder content and mean carbide grain size. Very interesting, length-scale effects on testing are observed in terms of dispersion of measured hardness value as applied load decreases. These findings, together with similar ones linked to length-scale influence on scratch response, point out that effective selection of mechanical testing parameters become critical for studying and understanding phenomena such as elastic/plastic and deformation/fracture transitions in AMed hardmetals.

1. Introduction

In recent decades, production of parts with complex geometries via traditional manufacturing from different types of advanced materials, such as high-temperature alloys, inorganic-base composites and ceramics, has become a relevant challenge. The main drawback is the need of extensive efforts in terms of process planning or post-processing to achieve the final product with the desired geometry. They could be overcome by means of Additive Manufacturing (AM), an emerging processing technology that offers the ability to shape components in complex geometries, unachievable with traditional methods while also reducing steps in the manufacturing process [1]. Tungsten carbide - cobalt (WC-Co) cemented carbides, usually referred to as hardmetals, are composite materials that could take profit from processing complex geometries via AM. The combination of different and complementary properties exhibited by their constitutive phases (hard WC grains and tough Co-base binder), together with the excellent wetting of Co on WC during the liquid phase sintering (relevant for the sinterability of final products) are main reasons for the outstanding performance exhibited by tools and components made from hardmetals [2].

AM is defined as a process of joining materials to make objects from 3D digital model data, usually layer upon layer, as opposed to subtractive manufacturing methodologies [3]. AM techniques can be divided in two broad categories: energy- and material-delivery routes. They can be differentiated due to their binding mechanisms and the feedstock morphology or delivery methods. Examples of energy-based routes are

* Corresponding author at: CIEFMA, Department of Materials Science and Engineering, Universitat Politècnica de Catalunya - BarcelonaTech, Campus Diagonal Besòs-EEBE, 08019 Barcelona, Spain.
E-mail address: laura.cabezas.i@upc.edu (L. Cabezas).

https://doi.org/10.1016/j.ijrmhm.2022.106099
Received 10 October 2022; Received in revised form 19 December 2022; Accepted 23 December 2022
Available online 25 December 2022

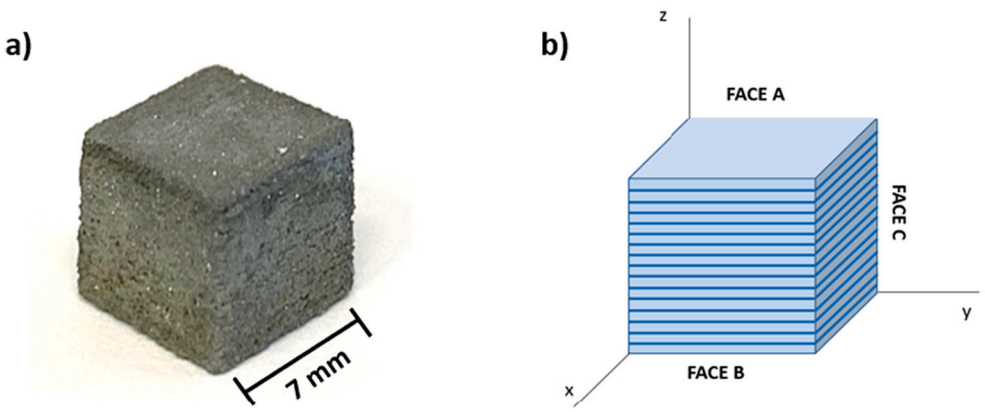

Fig. 1. (a) Image of the cubic 3D printed specimen, and (b) schematic representation of the three faces.

directed energy deposition, laser powder bed fusion and electron beam melting. Filament extrusion, binder jetting, material jetting and sheet lamination are representatives of material-delivery routes. In general, material-delivery methods follow the idea of Shaping-Debinding-Sintering as sequential processing route, which is the reason they are often refered to as "sinter-based" AM technologies [1].

Regarding hardmetals, a variety of AM technologies have been applied for processing different compositions since the early 2000s. Published research is mainly limited to WC-Co systems and exclusively aimed to tooling applications, attempting to reduce tool weight and enable internal cooling in the supporting structures (e.g. Refs. [4–19]), However, considering the extreme versatility of AM for introducing geometric complexity at both macro- and micrometric dimensions, innovative design and material control at every volume element, it is clear that potential range of application for hardmetals will significantly expand in coming years, particularly as wear parts to be implemented in mining, agriculture and food processing. Review of published literature shows that, in general, success has been variable. On the one hand, AM routes based on selective delivery of energy (mainly selective laser melting) have achieved sparse densification or properties (e.g. Refs. [10,16,20–29]). They have also highlighted the challenges involved in manufacturing fully dense WC-Co parts with satisfactory properties via laser sintering, indicating that the high-speed and local cycle of heating and solidification does not allow the typical liquid phase sintering step. Apart from densification, the exposure of WC-Co to high temperatures may cause decarburization of WC, the formation of carbides like W_2C and/or Co evaporation. Furthermore, internal (micro- and gradient) residual stresses, which adversely affect the properties of the final part, are often documented. On the other hand, AM technologies involving selective delivery of material (sinter-based AM), and particularly binder jetting (BJT), have yielded promising results for both hardmetals (e.g. Refs. [6,9,30]) and TiCN based cermets [30, 31]. In those cases, as expected, besides the need of dedicated feedstock and/or raw materials for the given AM technology, special care must be taken during post-processing (including debinding and sintering) to achieve the required microstructural scenario and mechanical properties. However, these post-processing steps should not be seen as a restriction of the process, since the amount of organic binder involved is quite small, as compared to those used in other shaping technologies, such as extrusion or powder injection moulding. From this perspective, limitations mainly arise from the minimal amount of Co needed to get dense samples, which are currently in the range of 10–12 wt%, and corresponding upper-level hardness values that may be achieved. Within the above context, it is evident that the full potential of AM technologies for hardmetals is still to be explored. In this regard, lack of information and need of further knowledge apply not only to processing issues but also to corresponding relationships between microstructure and mechanical integrity for AMed hardmetals.

Following the above ideas, it is the main objective of this work to study the correlation between microstructure and mechanical properties for a medium/coarse grained WC-12%wtCo hardmetal grade produced by BJT and subsequent sintering. However, different from previous literature studies, emphasis is here placed on identification and analysis of length-scale considerations on testing for effective measurement of its mechanical properties, mainly in terms of hardness and sliding contact (scratch) response at both macroscopic (global) and microscopic (local) levels. In doing so, special attention is paid to the influence of the effective ratio between characteristic lengths of contact-induced imprints/tracks and microstructure on the measured properties (mean and variability) as well as on the deformation/fracture micromechanisms involved.

2. Experimental aspects

2.1. Materials studied

Test specimens were printed in shapes of simple cubes (10*10*10 mm^3) using a spray dried and presintered WC-12%$_{wt.}$Co granulate without grain growth inhibitors (GGI), experimentally developed by Fraunhofer IKTS under reference WC12Co-2019. Powder employed had an apparent density of 4.73 g/cm^3 as well as a granule-size distribution described by the following percentiles: $d_{10} = 12.7$ μm, $d_{50} = 18.3$ μm, and $d_{90} = 29.2$ μm. It was used on a ZPrinter Z510 from 3D-Systems (former ZCorporation) with a layer thickness of 100 μm and a binder saturation of 150%. Debinding and sintering was done in an industrial-like sinterHIP furnace (FCT Systeme) at temperatures as high as 1500 °C and Ar pressure of 100 bar. The relatively high sintering temperatures used, in comparison to those commonly employed when sintering conventional green parts produced by uniaxial pressing, PIM or extrusion, were needed due to the lower green density of the printed parts. First trials with cubes sintered at 1450 °C did not achieve full densification. However, increasing the sintering temperature up to 1500 °C yielded 100% dense samples. Preliminary optical microscopy (OM) showed the existence of a relatively wide carbide size distribution, including a significant volume fraction of carbides larger than 3 μm. Although this was also discerned in the specimens consolidated in the first trials, it was more pronounced as sintering temperature was increased. Density and magnetic properties were measured according to ISO 3369 and 3326 and showed, next to full density, that a two-phase microstructure of WC and Co without any undesired eta phase or free graphite was achieved.

Microstructural and mechanical characterization was conducted in three out of the six faces of the cube, Fig. 1.a. The aim behind this approach was to study possible microstructural and mechanical changes derived from the process of depositing material layer by layer. Cube faces studied are referred to as: Face A in the x-y plane, Face B in the y-z plane, and Face C in the x-z, Fig. 1.b shows an schematic representation

Table 1
Scratch parameters (tip radius, applied load, speed and scratch length) used in the different tests conducted.

Type of load	Tip radius (μm)	Applied load (N)	Speed (mm/min)	Scratch length (mm)
Constant	20	1.0	0.6	0.6
	50	6.3		
	100	25.0		
Progressive	50	0–3.1	0.6	2.6
	100	0–12.5		
	200	0–50.0		

of the cubic sample and the three referred faces.

2.2. Evaluation of microstructural and mechanical properties

Microstructural characterization was carried out using a Zeiss Neon40 field emission scanning electron microscope (FESEM). Images were taken at different magnifications (x1000, x2000, x3000, x5000), aiming to capture changes in the heterogeneous nature of the microstructural scenario, as described below. Micrographs were then analyzed by an automated analysis image procedure, as proposed by Tarragó and co-workers [32]. Due to the high sintering temperature, abnormal growth of several carbide grains was observed. Then, fraction and size distribution of the coarse (larger than 3 μm) grains and the fine-grained matrix were determined separately.

Mechanical properties, mainly hardness and scratch resistance, were evaluated at different length scales. Vickers hardness tests were conducted using three different applied load levels: 10 Kgf (HV10) - macrohardness; 1Kgf (HV1) - between macro- and microhardness; and 100gf (HV0.1) - microhardness. In doing so, sets of indentations along the thickness of the face under consideration were performed. They were separated from each other by a distance about twice the diagonal of the residual imprint. Hence, number of indentations conducted in each case was variable, depending on the applied load, i.e. 130, 50 and 20 imprints under applied loads of 100gf, 1Kgf and 10Kgf respectively. Imprint diagonals for each load were observed and measured by OM and FESEM.

Scratch tests were carried out using a sliding contact unit (CSM Revetest) equipped with a force and depth sensor. They were performed under both constant and increasing applied load. Three Rockwell dia-

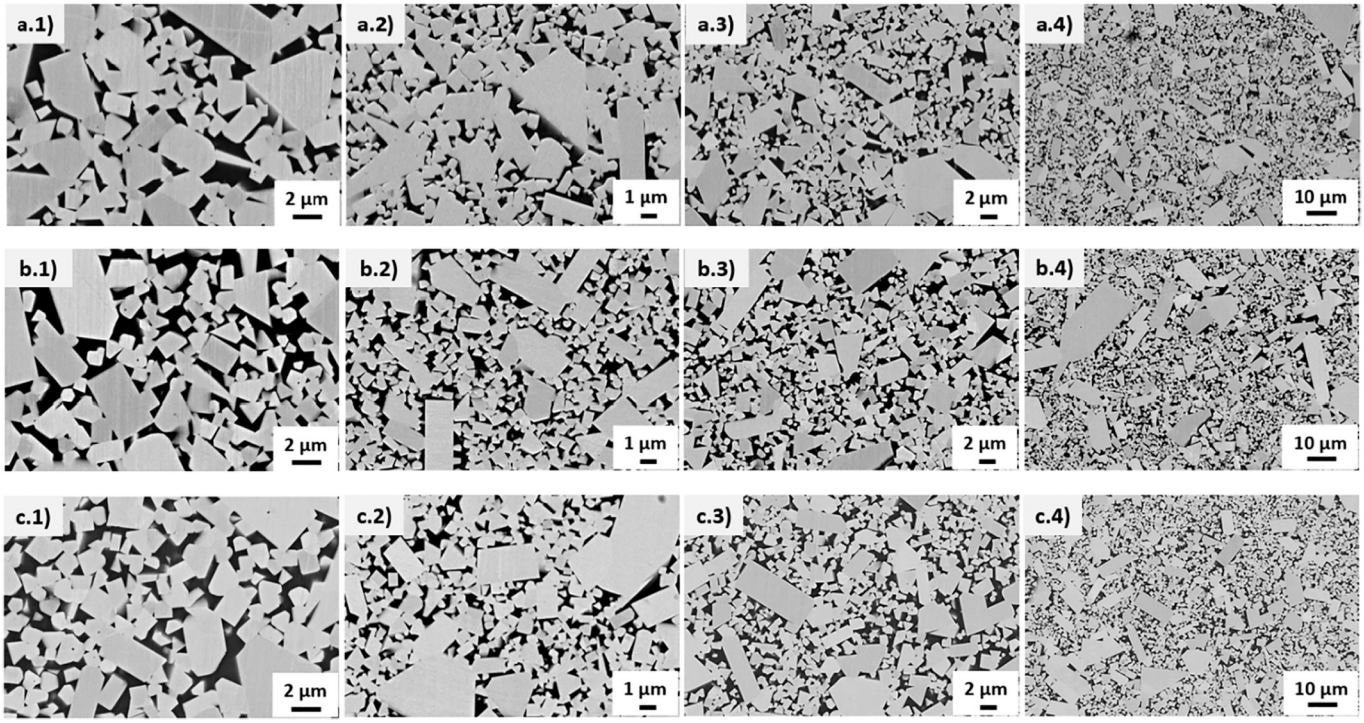

Fig. 2. Representative microstructures for each face: (a) Face A, (b) Face B and (c) Face C. For each face, study was conducted at four different magnifications.

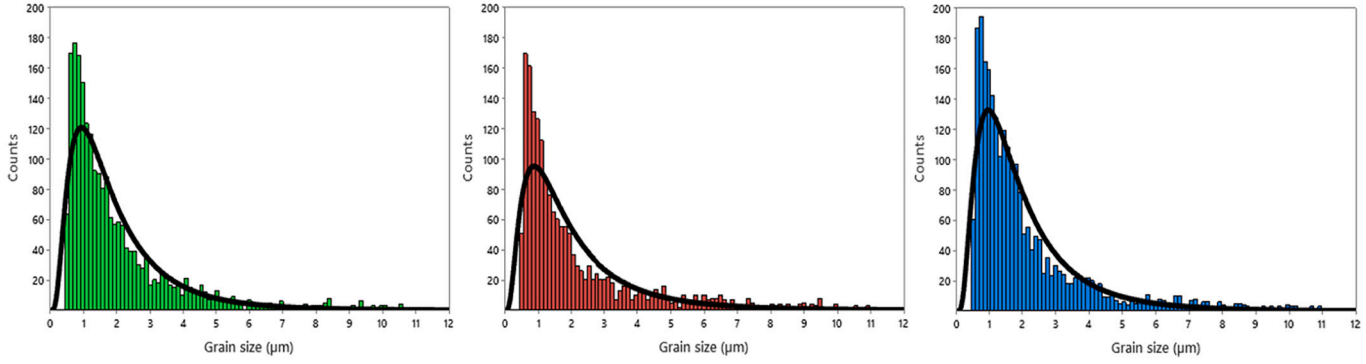

Fig. 3. Histograms and fitting curves for size distribution of carbide grains for: (a) Face A, (b) Face B, and (c) Face C.

Table 2
Mean and dispersion values for carbide grain size and relative volume fraction corresponding to small and large ceramic particles within each of the studied faces.

Face	Mean GS (matrix) (μm)	Volume fraction of matrix carbides (%)	Mean GS of large carbides (μm)	Volume fraction of large carbides (%)
A	1.2 ± 0.7	82.6	6.3 ± 3.7	17.4
B	1.0 ± 0.7	79.7	6.9 ± 3.8	20.3
C	1.2 ± 0.7	80.5	6.5 ± 3.8	19.5

Table 3
Hardness values measured on the three faces of the printed sample. For comparison purposes, similar data assessed on two reference WC-Co grades, consolidated by conventional pressing and sintering, are included.

Applied load	Face A	Face B	Face C	Ref. grade 1[a]	Ref. grade 2[b]
	H (GPa)	H (GPa)	H (GPa)	H (GPa)	H (GPa)
10 Kgf	12.0 ± 0.1	11.8 ± 0.3	12.1 ± 0.2	11.2 ± 0.1	11.0 ± 0.1
1 Kgf	12.9 ± 0.6	12.9 ± 0.6	12.6 ± 0.6	11.9 ± 0.2	11.9 ± 0.4
100 gf	13.6 ± 0.9	12.5 ± 1.2	12.2 ± 1.4	13.7 ± 0.4	12.9 ± 0.8

[a] WC-11%$_{wt.}$Co with a homogeneous microstructure, whose mean carbide grain size is about 1 μm.
[b] WC-7%$_{wt.}$Co with a homogeneous microstructure, whose mean carbide grain size is about 5 μm.

mond tips with different radius were employed (Table 1). Several combinations of applied load and tip radius values were implemented, aiming to attain damage scenarios with distinct characteristic length-scales. In doing so, effective values of sliding contact stresses were estimated by recalling scratch hardness definition, according to [33]:

$$H_S = F_N / A_s \quad (1)$$

where H_S is the scratch hardness (MPa), F_N is the applied normal load (N) and A_S is the sliding contact area (mm^2), the latter assumed to be semi-circular on the basis that tips exhibit sphero-conical geometries. This was helpful to evaluate and compare sliding contact stresses associated with applied loads and radius of tips used. Residual scratch grooves developed in all the sliding contact tests were observed and measured by means of OM and FESEM.

3. Results and discussion

3.1. Microstructural parameters

Fig. 2 shows representative images of the microstructural scenario discerned at different magnifications for the three faces. Corresponding grain size distributions are given in Fig. 3. Independent of the face under consideration, they are found to follow a logarithmical normal distribution. In this regard, it should be highlighted the significant number of grains with sizes between 3 and 10 μm. On this basis, the heterogeneous-like microstructure has been treated as consisting of two carbide populations: one corresponding to small carbides, referred as a carbide matrix (< 3 μm), and another one gathering all the large carbides (> 3 μm). Table 2 reports values of mean and standard deviation for carbide grain size, as well as relative volume fraction that represent every carbide group in each face. In general, there are no significant differences among listed values, indicating the isotropic-like character expected from BJT materials. The relatively high fraction of large carbides evidenced in all faces may be rationalized by the absence of any GGI addition together with the high sintering temperature used for full densification of the studied specimen. As a final result, the microstructural scenario may be described as consisting of a wide WC grain size distribution with a significant volume fraction of carbides higher than 3 μm. Consequently, it may affect mechanical property measurements, depending on length-scale under consideration, as will be shown later.

Table 4
Hardness imprint's diagonal, and corresponding ratios between such value and sizes of small and large carbides, resulting from tests conducted on the three faces of the AM specimen.

Applied load		10 Kgf	1 Kgf	0.1 Kgf
Face A	Diagonal (μm)	123.0 ± 0.5	37.6 ± 0.8	11.6 ± 0.4
	Diagonal/Carbide$_{small}$	102.5	31.3	9.7
	Diagonal/Carbide$_{large}$	19.5	6.0	1.8
Face B	Diagonal (μm)	124.0 ± 1.6	37.6 ± 0.8	12.1 ± 0.6
	Diagonal/Carbide$_{small}$	124.0	37.6	12.1
	Diagonal/Carbide$_{large}$	18.0	5.4	1.8
Face C	Diagonal (μm)	122.9 ± 1.0	38.1 ± 0.9	12.3 ± 0.7
	Diagonal/Carbide$_{small}$	102.4	31.8	10.3
	Diagonal/Carbide$_{large}$	18.9	5.9	1.9

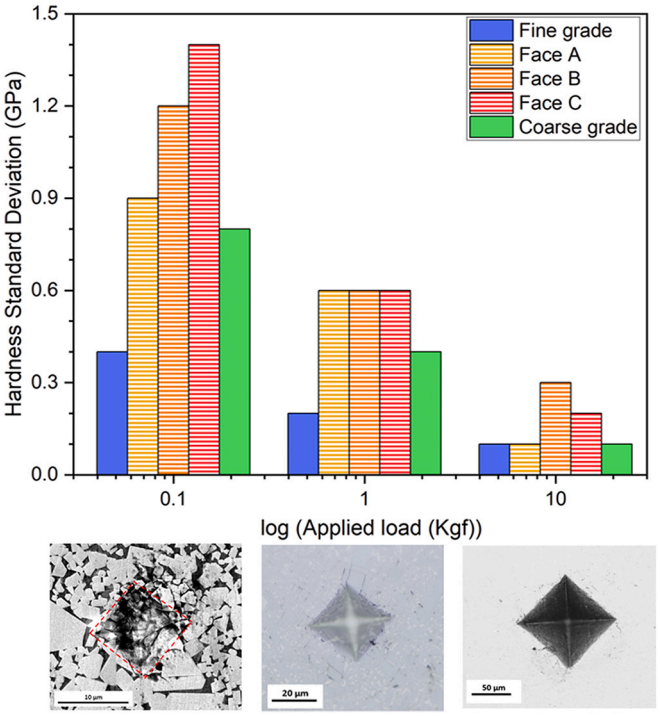

Fig. 4. Dispersion of hardness values for tests conducted in each face as a function of the applied load (log scale) during Hardness Vickers test. Representative images of imprints resulting from tests conducted at different load values are also given. Data measured on reference fine- and coarse-grained hardmetal grades with homogeneous microstructures are included too, for comparison purposes.

3.2. Vickers hardness tests

Hardness results are listed in Table 3. For comparison purposes, values measured under similar testing conditions for two commercial hardmetal grades with homogeneous microstructures are also included. These reference materials correspond to WC-11%$_{wt.}$Co and a WC-7%$_{wt.}$Co materials with mean carbide grain size of 1 μm and 5 μm, respectively, which have been consolidated following a conventional pressing and sintering route. As it was found from microstructural characterization, mean hardness values are similar for the three faces studied, giving additional support to the statement that specimen

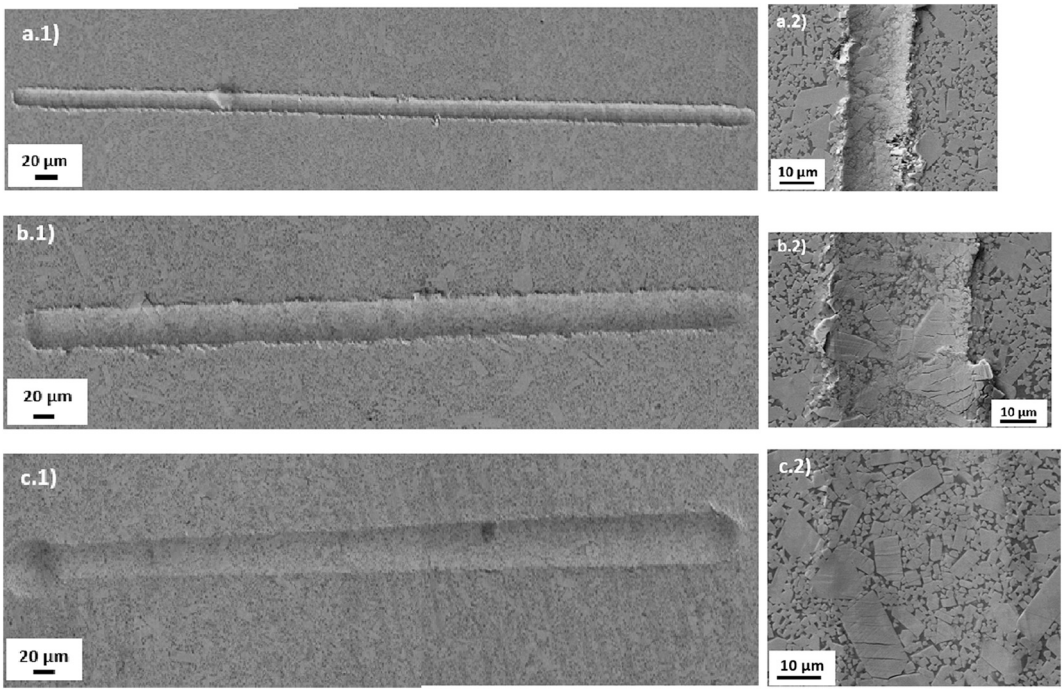

Fig. 5. Scratch tracks resulting from constant-load tests in Face A: (a.1) 20 µm tip and applied load of 1 N, (b.1) 50 µm tip and applied load of 6.25 N, and (c.1) 100 µm tip and applied load of 25 N. High-magnification images of specific regions within the groove surface are given in (a.2), (b.2) and (c.2).

studied is isotropic. Furthermore, they are in satisfactory agreement with those reported in the literature for hardmetals with similar microstructural assemblage [6,17,34]. Although relatively higher values are measured for lower applied loads, i.e. 100 gf and 1 Kgf, than for the highest imposed one, i.e. 10Kgf, there is not any clear size indentation effect on hardness mean value. It is speculated that it could be expected to emerge for even lower applied indentation loads. However, and very interesting, there are clear length-scale effects regarding standard deviation of the measured hardness values. The lower the applied load, the higher the scatter of hardness values, the latter rising from 1% to 10% when the former decreases from 10 Kgf to 100 gf. Such findings are the compromising result of lower ratios between diagonal impression and microstructural characteristic lengths, as applied load diminishes. Such trend is clearly supported by the results listed in Table 4 and shown in Fig. 4, where it may be discerned that residual imprints at the lowest studied load are of similar length-scale to the size of larger carbides identified in the microstructure. Meanwhile, it may be stated that as far as imprints are higher than 10 times such microstructural parameter, hardness values do reflect typical mechanical response of the composite material, independent of the location where that property is assessed. Previous analysis is supported by hardness data collected from similar testing program conducted for two commercial reference grades with homogenous microstructures. On the one hand, for relatively low applied loads (0.1 and 1 Kgf), hardness dispersion measured for the coarser reference grade is higher than for the finer one. On the other hand, independent of applied indentation load, hardness dispersion values measured on the materials with homogeneous microstructures are always lower than those assessed on the BJT one. This experimental fact is quite interesting for further research on AMed materials, as it may be key to propose and define testing parameters for assessment of mechanical properties of heterogeneous microstructures as well as regions where interlayer or interface-related issues may exist.

3.3. Scratch tests under constant load

Sliding contact tests conducted under constant load were implemented to assess deformation, damage and fracture features associated with different stress levels. In this regard, specific combinations of applied load and tip radius were chosen to impose similar sliding contact stresses, as listed in Table 1. Representative scratch tracks resulting from constant load tests conducted are shown in Fig. 5.a, 5.b and 5.c. Lower tip radius yielded smaller groove sizes, although linked to pronounced surface damage levels. The latter was the case for all scratch tests conducted using 20 µm and 50 µm tips, although under different applied loads, where huge plastic deformation was discerned within the cobalt binder together with cracked or even smashed WC particles all along the track (e.g., Fig. 5.a.2 and 5.b.2). Such similar scenario was expected because ratio between applied loads is 6.25 in both tests, i.e. same value as the one corresponding to square of the relative differences in tip radius. Meanwhile, similar equivalent stress state was not effectively imposed with the indenter with 100 µm tip radius used, even though applied load ratios were varied accordingly. This is reflected by the lower damage level evidenced within the scratch track, and mainly concentrated in the existing large carbide particles (Fig. 5.c.2). Such distinct behavior should be related to sharp-blunt transition linked to indenter tips used and would be expected to be dependent on the microstructural and mechanical characteristics of the hardmetal grade under consideration. Hence, this may be identified as an additional testing parameter to explore for accurate and reliable assessment of mechanical properties of AMed hardmetals in future research.

3.4. Scratch tests under progressive load

Sliding contact tests under progressive load were carried out up to maximum load values about half of those used in previously described constant-load scratches. The main idea behind it was to document and identify damage emergence and evolution, using indenter tips for which relevant damage had been evidenced before. Within this context, representative scratch tracks resulting from progressive load tests are shown in Fig. 6.a, 6.b and 6.c, for 50 µm, 100 µm and 200 µm tips respectively. Tests using the 20 µm tip were not run. Instead, a more curved tip (200 µm of radius) was included in the testing program. Load was gradually increased within a relatively long distance, about four times the one used in constant-load scratches.

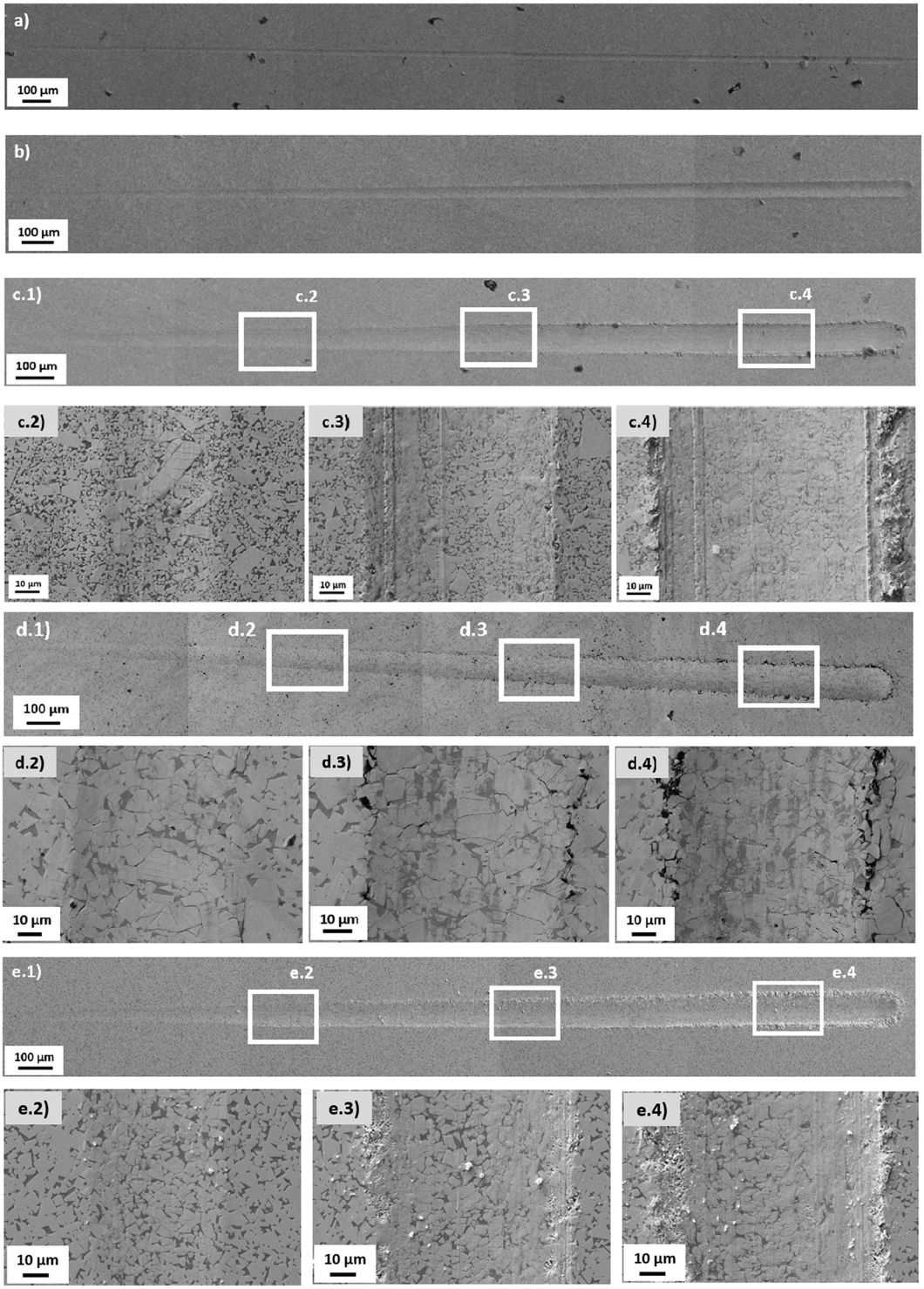

Fig. 6. Scratch tracks resulting from progressive-load tests in Face A: (a) 50 µm tip and applied load from 0 N to 3.125 N, (b) 100 µm tip and applied load from 0 N to 12.5 N and (c.1) 200 µm tip and applied load from 0 N to 50 N. For comparison purposes, scratch tracks resulting from progressive-load tests with 200 µm tip in reference hardmetal grades with homogeneous microstructures: (d.1) coarse grade, and (e.1): fine grade, are also included. High-magnification images corresponding to specific regions within the groove surface resulting from tests run with the 200 µm tip are given in (c.2), (c.3) and (c.4) for Face A, (d.2), (d.3) and (d.4) for reference coarse-grained grade, and (e.2), (e.3) and (e.4) for reference fine-grained grade.

It is clear that maximum applied load in scratch tests using the 50 µm tip translates into very low stresses which induce just slight plastic deformation. Indeed, tracks resulting from applying constant or progressive loads, at least within the range here used, are somehow similar. Meanwhile, use of higher load ranges with 100 µm and 200 µm tips (Fig. 6.b. and 6.c.1) allowed to discern emergence and evolution of damage. As before, for comparison purposes, similar progressive load scratch tests were performed on the fine- and coarse-grained hardmetal grades with homogenous microstructures (see Section 3.2). Fig. 6.d.1 and 6.e.1 show the resulting tracks. It may be evidenced that first damage event discerned in BJT material was cracking of large carbides (Fig. 6.c.2), in complete agreement with the early damage features

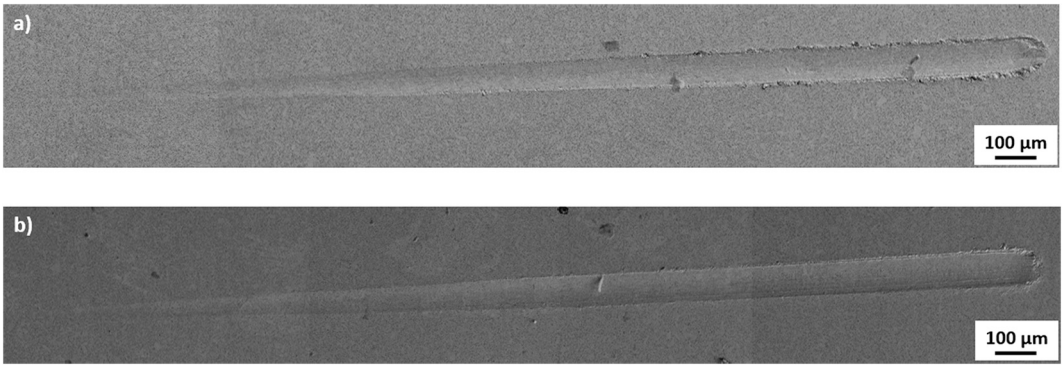

Fig. 7. Scratch tracks resulting from progressive-load tests with 200 µm tip and applied load from 0 N to 50 N: (a) Face B and (b) Face C.

found for the reference coarse-grained hardmetal (Fig. 6.d.2). Afterwards, damage evolution takes place by combining compatible plastic deformation between both phases with localized microfracture within contiguous carbide grains. The former is in concordance with the damage scenario found within the track of the reference fine-grained hardmetal under the same level of applied load, (Fig. 6.e.3), whereas the latter is directly related to the intrinsic cracking evolution experienced by the coarse carbides, as observed for the corresponding reference material (Fig. 6.d.3). Finally, the last contact-related mechanism observed was the re-embedment of WC fragments into the deformed binder phase, as it was also the case for both reference hardmetal grades at such high levels of applied load (Fig. 6.c.4, 6.d.4 and 6.e.4). Indeed, final damage scenario is quite similar to the one evidenced in the constant-load tests conducted using the 20 µm tip under an applied load of 1 N.

As it was the case for Vickers hardness tests, it is worth mentioning that no significant differences were observed among the scratch tracks performed on the distinct faces of the printed specimen, as it is shown in Fig. 6.c.1 and Fig. 7. Hence, once again, the isotropic-like nature of BJT specimens is confirmed, regarding mechanical respose under sliding contact conditions. This finding, together with the fact that hardness and scratch resistance results are in complete agreement with those reported by other authors on conventionally pressed and sintered WC-Co grades with different microstructural assemblages (e.g. Ref [35–37]) may be assessed as a positive one in terms of wear-related applications. However, special care should be taken on extrapolating this conclusion to other mechanical properties, such as strength; and thus, to other applications, such as cutting tools. In these cases, the heterogeneous nature of the microstructure exhibited by the BJT cemented carbide investigated would surely result in lower strength values, because the detrimental role expected to be played by large carbides as critical failure sites. On this account, it should be indicated that this study is currently being extended to other BJT hardmetals with different compositions, namely WC-12%$_{wt.}$Co and WC-17%$_{wt.}$Co samples, produced by IKTS without exhibiting such relatively wide carbide grain size distribution, and the results of such work will be presented in future publications.

4. Conclusions

Based on the results obtained from microstructural and mechanical characterization of a hardmetal manufactured by BJT and subsequebtly sintered, the following conclusions may be drawn:

(1) WC-12%wtCo-2019 sample without GGI processed by means of BJT exhibits a microstructure consisting of a relatively high volume content (about 18–20%) of carbide grains larger than 3 µm together with a predominant population of fine ones. This heterogeneous-like microstructural scenario is similar for the three faces studied, and is directly linked to the relatively high sintering temperature needed for getting full dense specimens manufactured following this AM route. Further optimization of processing and sintering is expected to result in suppression of any abnormal growth of some carbides.
(2) Mechanical characterization, in terms of hardness and sliding contact response, indicates that BJT hardmetal studied exhibits an isotropic-like behavior, with hardness and scratch resistance values in agreement with those reported in the literature for cemented carbides with similar microstructural assemblage.
(3) Interesting length-scale effects on testing are observed, mainly in terms of dispersion of the measured hardness values as applied load decreases; and thus, characteristic lengths of residual impression and microstructure – particularly regarding abnormally (size higher than 3 µm) large carbides - become similar.
(4) Scratch tests conducted using tips of different curvature and under constant and/or progressive loads allow to impose similar sliding contact stresses but linked to tracks of different length scales. Although experimental data gathered is rather limited, preliminary results indicate that effective selection of scratch testing parameters may be key for studying the influence of sharp/blunt character of used tips on elastic/plastic and deformation/fracture transitions in hardmetals as a function of their microstructural characteristics.

Declaration of Competing Interest

The authors declare that they have no known competing financial interests or personal relationships that could have appeared to influence the work reported in this paper.

Data availability

The data that has been used is confidential.

Acknowledgements

This work was supported by the Spanish Ministerio de Ciencia e Innovación MICINN – FEDER (Spain) through Grant PID2019-106631GB-C41 (AEI/10.13039/501100011033). L. Cabezas acknowledges the Ph.D. scholarship received from the Spanish Ministerio de Ciencia e Innovación MICINN – FEDER (Spain), through Grant PRE2020-092445. The study has been conducted in the framework of a bilateral research collaboration between Fraunhofer Institute for Ceramic Technologies and Systems IKTS and Universitat Politécnica de Catalunya – CIEFMA.

References

[1] A. Mostafaei, A.M. Elliott, J.E. Barnes, F. Li, W. Tan, C.L. Cramer, P. Nandwana, M. Chmielus, Binder jet 3D printing—process parameters, materials, properties,

modeling, and challenges, Prog. Mater. Sci. 119 (2021), 100707, https://doi.org/10.1016/j.pmatsci.2020.100707.
[2] J. García, V. Collado Ciprés, A. Blomqvist, B. Kaplan, Cemented carbide microstructures: a review, Int. J. Refract. Met. Hard Mater. 80 (2019) 40–68, https://doi.org/10.1016/j.ijrmhm.2018.12.004.
[3] ISO/ASTM 52900, Additive Manufacturing - General Principles - Terminology, Int. Stand, 2015.
[4] J. Pötschke, C. Berger, H.J. Richter, U. Scheithauer, S. Weingarten, Additive Manufacturing of Hardmetals, Proceedings of Euro PM 2017 Congress and Exhibition, Ed, EPMA, Milan, Italy, 2017.
[5] U. Scheithauer, J. Pötschke, S. Weingarten, E. Schwarzer, A. Vornberger, T. Moritz, A. Michaelis, Droplet-based additive manufacturing of hard metal components by thermoplastic 3D printing (T3DP), J. Ceram. Sci. Technol. 8 (2017) 155–160, https://doi.org/10.4416/JCST2016-00104.
[6] R.K. Enneti, K.C. Prough, T.A. Wolfe, A. Klein, N. Studley, J.L. Trasorras, Sintering of WC-12%Co processed by binder jet 3D printing (BJ3DP) technology, Int. J. Refract. Met. Hard Mater. 71 (2018) 28–35, https://doi.org/10.1016/j.ijrmhm.2017.10.023.
[7] K.S. Prakash, T. Nancharaih, V.V.S. Rao, Additive manufacturing techniques in manufacturing -an overview, Mater. Today Proc. 5 (2018) 3873–3882, https://doi.org/10.1016/j.matpr.2017.11.642.
[8] W. Lengauer, I. Duretek, M. Fürst, V. Schwarz, J. Gonzalez-Gutierrez, S. Schuschnigg, C. Kukla, M. Kitzmantel, E. Neubauer, C. Lieberwirth, V. Morrison, Fabrication and properties of extrusion-based 3D-printed hardmetal and cermet components, Int. J. Refract. Met. Hard Mater. 82 (2019) 141–149, https://doi.org/10.1016/j.ijrmhm.2019.04.011.
[9] C.L. Cramer, P. Nandwana, R.A. Lowden, A.M. Elliott, Infiltration studies of additive manufacture of WC with Co using binder jetting and pressureless melt method, Addit. Manuf. 28 (2019) 333–343, https://doi.org/10.1016/j.addma.2019.04.009.
[10] J. Chen, M. Huang, Z.Z. Fang, M. Koopman, W. Liu, X. Deng, Z. Zhao, S. Chen, S. Wu, J. Liu, W. Qi, Z. Wang, Microstructure analysis of high density WC-Co composite prepared by one step selective laser melting, Int. J. Refract. Met. Hard Mater. 84 (2019), 104980, https://doi.org/10.1016/j.ijrmhm.2019.104980.
[11] C. Berger, J. Abel, J. Pötschke, T. Moritz, Properties of additive manufactured hardmetal components produced by fused filament fabrication (FFF), in: Proceedings of Euro PM 2018 Congress and Exhibition, Ed, EPMA, Bilbao, Spain, 2018.
[12] E. Carreño-Morelli, P. Alveen, S. Moseley, M. Rodriguez-Arbaizar, K. Cardoso, Three-dimensional printing of hard materials, Int. J. Refract. Met. Hard Mater. 87 (2020) 105110, https://doi.org/10.1016/j.ijrmhm.2019.105110.
[13] A. Aramian, S.M.J. Razavi, Z. Sadeghian, F. Berto, A review of additive manufacturing of cermets, Addit. Manuf. 33 (2020) 101130, https://doi.org/10.1016/j.addma.2020.101130.
[14] M. Padmakumar, Additive manufacturing of tungsten carbide hardmetal parts by selective laser melting (SLM), selective laser sintering (SLS) and binder jet 3D printing (BJ3DP) techniques, Lasers Manuf. Mater. Process. 7 (2020) 338–371, https://doi.org/10.1007/s40516-020-00124-0.
[15] T. Rieger, T. Schubert, J. Schurr, M. Butschle, M. Schwenkel, T. Bernthaler, G. Schneider, Slurry development for lithography-based additive manufacturing of cemented carbide components, Powder Technol. 383 (2021) 498–508, https://doi.org/10.1016/j.powtec.2021.01.049.
[16] O.D. Jucan, R.V. Gădălean, H.F. Chicinaș, M. Hering, N. Bâlc, C.O. Popa, Study on the indirect selective laser sintering (SLS) of WC-Co/PA12 powders for the manufacturing of cemented carbide parts, Int. J. Refract. Met. Hard Mater. 96 (2021) 2–10, https://doi.org/10.1016/j.ijrmhm.2021.105498.
[17] M. Mariani, I. Goncharov, D. Mariani, G. Pietro De Gaudenzi, A. Popovich, N. Lecis, M. Vedani, Mechanical and microstructural characterization of WC-Co consolidated by binder jetting additive manufacturing, Int. J. Refract. Met. Hard Mater. 100 (2021), 105639, https://doi.org/10.1016/j.ijrmhm.2021.105639.
[18] J.Y. Tang, L.M. Luo, Z. Liu, X. Zan, Y.C. Wu, Shape retention of cemented carbide prepared by Co melt infiltration into un-sintered WC green parts made via BJ3DP, Int. J. Refract. Met. Hard Mater. 107 (2022), 105904, https://doi.org/10.1016/j.ijrmhm.2022.105904.
[19] H. Kim, J. Il Kim, Y. Do Kim, H. Jeong, S.S. Ryu, Material extrusion-based three-dimensional printing of WC–Co alloy with a paste prepared by powder coating, Addit. Manuf. 52 (2022), https://doi.org/10.1016/j.addma.2022.102679.
[20] D. Gu, W. Meiners, Microstructure characteristics and formation mechanisms of in situ WC cemented carbide based hardmetals prepared by selective laser melting, Mater. Sci. Eng. A 527 (2010) 7585–7592, https://doi.org/10.1016/j.msea.2010.08.075.
[21] E. Uhlmann, A. Bergmann, W. Gridin, Investigation on additive manufacturing of tungsten carbide-cobalt by selective laser melting, Proc. CIRP 35 (2015) 8–15, https://doi.org/10.1016/j.procir.2015.08.060.
[22] R.S. Khmyrov, V.A. Safronov, A.V. Gusarov, Obtaining crack-free WC-Co alloys by selective laser melting, Phys. Procedia 83 (2016) 874–881, https://doi.org/10.1016/j.phpro.2016.08.091.
[23] I. Konyashin, H. Hinners, B. Ries, A. Kirchner, B. Klöden, B. Kieback, R.W.N. Nilen, D. Sidorenko, Additive manufacturing of WC-13%Co by selective electron beam melting: achievements and challenges, Int. J. Refract. Met. Hard Mater. 84 (2019), 105028, https://doi.org/10.1016/j.ijrmhm.2019.105028.
[24] C.W. Li, K.C. Chang, A.C. Yeh, On the microstructure and properties of an advanced cemented carbide system processed by selective laser melting, J. Alloys Compd. 782 (2019) 440–450, https://doi.org/10.1016/j.jallcom.2018.12.187.
[25] H. Ibe, Y. Kato, J. Yamada, M. Kato, A. Suzuki, N. Takata, M. Kobashi, Controlling WC/Co two-phase microstructure of cemented carbides additive-manufactured by laser powder bed fusion: effect of powder composition and post heat-treatment, Mater. Des. 210 (2021), 110034, https://doi.org/10.1016/j.matdes.2021.110034.
[26] T. Schwanekamp, G. Marginean, M. Reuber, A. Ostendorf, Impact of cobalt content and grain growth inhibitors in laser-based powder bed fusion of WC-Co, Int. J. Refract. Met. Hard Mater. 105 (2022), 105814, https://doi.org/10.1016/j.ijrmhm.2022.105814.
[27] E. Molobi, N. Sacks, M. Theron, Crack mitigation in laser engineered net shaping of WC-10wt%FeCr cemented carbides, Addit. Manuf. Lett. 2 (2022), 100028, https://doi.org/10.1016/j.addlet.2022.100028.
[28] L. Zhang, C. Hu, Y. Yang, R.D.K. Misra, K. Kondoh, Y. Lu, Laser powder bed fusion of cemented carbides by developing a new type of Co coated WC composite powder, Addit. Manuf. 55 (2022), 102820, https://doi.org/10.1016/j.addma.2022.102820.
[29] S. Fries, A. Vogelpoth, A. Kaletsch, C. Broeckmann, Influence of post heat treatment on microstructure and fracture strength of cemented carbides manufactured using laser-based additive manufacturing, Int. J. Refract. Met. Hard Mater. 111 (2023), 106085, https://doi.org/10.1016/j.ijrmhm.2022.106085.
[30] J. Pötschke, C. Berger, H.-J. Richter, T. Moritz, 3D-Binder-Jetting von Hartmetallen, wt Werkstattstech. Online 107 (2017) 439–440, https://doi.org/10.37544/1436-4980-2017-06-55.
[31] C. Berger, J. Pötschke, M. Fries, T. Moritz, A. Michaelis, Binder-jetting of TiCN-based cermets, Powder Metall. 65 (2022) 382–389, https://doi.org/10.1080/00325899.2022.2099636.
[32] J.M. Tarragó, D. Coureaux, Y. Torres, F. Wu, I. Al-Dawery, L. Llanes, Implementation of an effective time-saving two-stage methodology for microstructural characterization of cemented carbides, Int. J. Refract. Met. Hard Mater. 55 (2016) 80–86, https://doi.org/10.1016/j.ijrmhm.2015.10.006.
[33] J.D. Kamminga, P.F.A. Alkemade, G.C.A.M. Janssen, Scratch test analysis of coated and uncoated nitrided steel, Surf. Coat. Technol. 177–178 (2004) 284–288, https://doi.org/10.1016/j.surfcoat.2003.09.006.
[34] R.K. Enneti, K.C. Prough, Wear properties of sintered WC-12%Co processed via binder jet 3D printing (BJ3DP), Int. J. Refract. Met. Hard Mater. 78 (2019) 228–232, https://doi.org/10.1016/j.ijrmhm.2018.10.003.
[35] M.G. Gee, L. Nimishakavi, Model single point abrasion experiments on WC/Co hardmetals, Int. J. Refract. Met. Hard Mater. 29 (2011) 1–9, https://doi.org/10.1016/j.ijrmhm.2010.04.009.
[36] J.C.P. Zuñega, M.G. Gee, R.J.K. Wood, J. Walker, Scratch testing of WC/Co hardmetals, Tribol. Int. 54 (2012) 77–86, https://doi.org/10.1016/j.triboint.2012.02.027.
[37] Y.F. Zheng, G. Fargas, H. Besharatloo, M. Serra, J.J. Roa, E. Armelin, O. Lavigne, L. Llanes, Assessment of corrosion-induced changes on the mechanical integrity of cemented carbides at small length scales, Int. J. Refract. Met. Hard Mater. 84 (2019), 105033, https://doi.org/10.1016/j.ijrmhm.2019.105033.